JOURNAL OF PROPULSION AND POWER
Vol. 20, No. 4, July–August 2004

Time-Resolved Fuel-Grain Port Diameter Measurement in Hybrid Rockets

Shane De Zilwa,* Gregory Zilliac,† and Michael Reinath‡
NASA Ames Research Center, Moffett Field, California 94035
and
Arif Karabeyoglu§
Stanford University, Stanford, California 94305

A novel technique is presented for determining the instantaneous spatially averaged port diameter of solid-fuel grains in hybrid rocket motors. This technique requires measurement of the frequency of the Helmholtz oscillation of the motor and is based on the principle that this frequency is inversely proportional to the square root of the chamber volume. This technique was applied to a hybrid rocket motor burning paraffin wax with gaseous oxygen. The calculated variation of port diameter agreed well with the correlation for average regression rate, determined from mass loss during operation. A major advantage is that the only instrumentation required for implementing this technique is a high-speed pressure transducer or a photomultiplier tube.

Nomenclature

A	=	throat area
a	=	fuel regression rate law coefficient
c	=	speed of sound
D	=	port diameter of the fuel grain
F	=	longitudinal mode frequency
f	=	Helmholtz frequency
G	=	oxidizer mass flux through the port
L	=	length of the fuel grain
L'	=	total combustor length
l	=	effective length of the throat
l'	=	length of the throat
M	=	acoustic-wave multiple
$\dot{m}$	=	oxidizer mass flow rate
n	=	fuel regression rate law exponent
P	=	chamber pressure
$\dot{r}$	=	fuel regression rate
t	=	time
V	=	chamber volume
V'	=	postcombustion-chamber volume

Subscripts

av	=	average
f	=	final
s-av	=	spatially averaged
tot	=	total
0	=	initial
1	=	at time of first frequency measurement, $t = 0.5$ s

Received 28 May 2003; presented as Paper 2003-4595 at the AIAA/ASME/SAE/ASEE 39th Joint Propulsion Conference, Huntsville, AL, 20 July 2003; revision received 24 September 2003; accepted for publication 3 December 2003.

*National Research Council Associate; currently Postdoctoral, Sandia National Laboratories Combustion Research Facility, Livermore, California. Member AIAA.
†Research Scientist.
‡Research Scientist. Member AIAA.
§Research Associate, Department of Aeronautics and Astronautics. Member AIAA.

Introduction

THE most important measurement in characterizing a hybrid-rocket propellant is the spatially averaged burning, or regression, rate of the solid-fuel grain. The regression rate of hybrid fuels can be dependent on many system parameters including oxidizer mass flux, chamber pressure, and axial distance along the grain.[1–5] Usually the regression rate is determined as a time-averaged value from the mass lost from the grain over the duration of the burn, with corrections for the ignition and shutdown transients, and this technique is referred to as the end-point technique.[6]

A series of over 70 tests, using paraffin wax and gaseous oxygen, in which the average fuel regression rate was determined using the end-point technique, showed that, over the range of system parameters considered, the fuel regression was uniform over the length of the grain, independent of pressure and related to the oxidizer mass flux by the expression:

$$\dot{r} = a \cdot G^n \tag{1}$$

where a and n are 0.117×10^{-3} m/s $(\text{kg/m}^2 \cdot \text{s})^{-n}$ and 0.62, respectively.[7,8] These regression rates are around three to five times that of traditional hybrid fuels such as high-density polyethylene, polymethyl methacrylate, and hydroxil-terminated polybutadine.

Because of the dependence of the fuel regression rate on the oxidizer mass flux, as the port diameter changes during the burn, so do the instantaneous oxidizer mass flux and fuel regression rate. Therefore, time-resolved measurement of regression rate is desirable and, if done properly, could minimize the uncertainties associated with the ignition and shutdown transients. A time-resolved measurement would also provide a means for obtaining multiple data points from a single test, thus, reducing the time and cost involved with testing. A final important application of time-resolved measurement of fuel-grain port diameter regression is in real-time vehicle health monitoring.

Techniques for obtaining time-resolved measurement of port diameter included ballistic reconstruction of the complete regression history,[6] which has been shown to be more accurate than the end-point technique and provides many of the potential advantages of a time-resolved measurement. Ballisic reconstruction does, however, require knowledge of the final fuel-grain diameter before it can be implemented and, hence, cannot be used for real-time measurement. Time-resolved regression of hybrid-fuel grains has also been obtained, through measurement of the instantaneous thickness or port diameter, with ultrasound[5,9,10] and x-ray radiography.[5,11] These techniques have the potential to provide real-time measurements but require specialized instrumentation.

This paper presents a novel method for calculating the instantaneous spatially averaged port diameter of the grain from analysis of a high-speed pressure transducer signal. It is based on the principle that the frequency of the Helmholtz oscillation decreases in a predictable manner as the port diameter of the grain increases during the burn. The technique is applied to a hybrid-rocket burning paraffin wax with gaseous oxygen, and the results are compared with the following expression for instantaneous port diameter:

$$D^{2n+1} - D_0^{2n+1} = 2a(2n+1)(4\dot{m}/\pi)^n t \qquad (2)$$

which was obtained by integrating the regression-rate correlation of Eq. (1), with the assumptions that the oxidizer mass flow rate is constant and that the end faces of the fuel grain do not burn. The ability to obtain the same information nonintrusively by observing the plume with a photomultiplier is also considered.

The flow configuration and instrumentation are described in the next section, followed by presentation of the method for calculating the instantaneous port diameter of the fuel grain and evaluation of the results. The paper ends with a summary of the most important conclusions.

Flow Configuration and Instrumentation

A simplified schematic of the facility used for the experiments is shown in Fig. 1. It consists of a gaseous oxygen delivery system, an ignition system, and a combustion chamber. During operation of the facility, the pressure upstream of a sonic orifice is maintained constant by a feedback-driven control valve. Therefore, a constant oxygen mass flow rate that is decoupled from pressure fluctuations in the combustion chamber is established downstream of the orifice.

The 1.2-m-long fuel grain, consisting of cast wax in a paper-phenolic tube, is located within the steel combustion chamber. The grain has an outer diameter of 0.195 m, and the inner diameter is chosen to provide the desired average mass flux for a particular test. The downstream end of the combustion chamber is constricted by a converging graphite nozzle, the throat diameter of which is chosen to provide the desired chamber pressure.

Combustion is initiated by heating the main oxygen flow with an igniter system that consists of a methane–oxygen stream that is ignited by two spark plugs. The igniter system is switched off after 0.3 s. The paraffin-based fuel and oxygen then burn, and the combustion products are exhausted through the nozzle. The experiments explored oxygen flow rates of 2 and 6 kg/s and chamber pressures between 150 and 600 psi (1.03 and 4.14 MPa). The average mass flux ranged between 100 and 400 kg/m$^2 \cdot$ s^{-1}, with corresponding initial mass fluxes of between 200 and 1000 kg/m$^2 \cdot$ s^{-1}, and are equivalent to those in a moderate-sized flight motor.

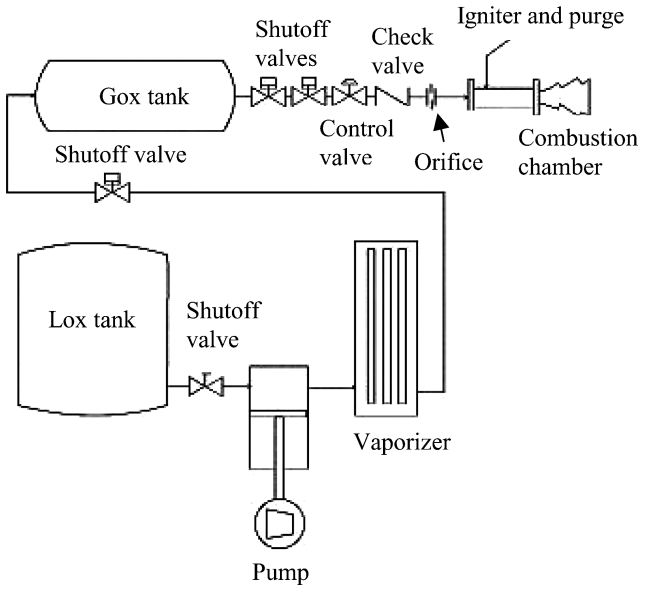

Fig. 1 Simplified schematic of the combustion facility.

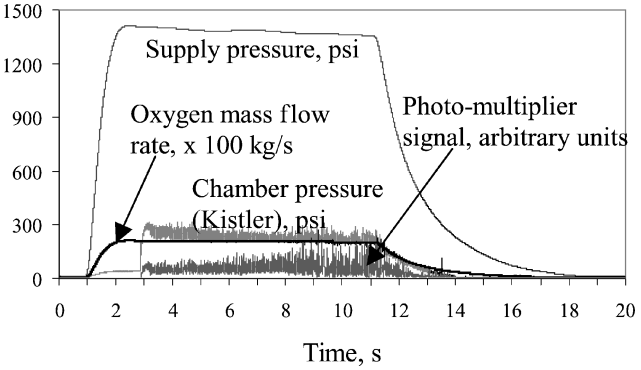

Fig. 2 Data acquired during operation: $P_{av} = 300$ psi (2.07 MPa), $\dot{m}_{av} = 2.05$ kg/s, $OFR_{av} = 1.70$, and $D_0 = 0.090$ m.

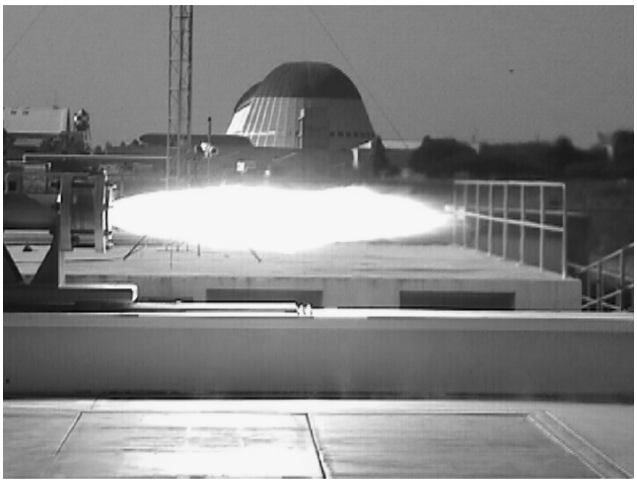

Fig. 3 Typical plume.

Parameters recorded during operation include the supply and chamber pressures measured by slow-response inert-liquid-filled pressure transducers (Rosemount 1151GP9E2AB2P2 and 1151GP9M2AB2P2, respectively) and the oxygen mass flow rate as deduced from flow through a choked orifice. The chamber pressure was also measured with a fast-response piezoelectric transducer (Kistler 601B1 with charge amplifier 5010B), and the plume flicker was measured with a photomultiplier (Thorn EMI 9818B). These two measurements are the most important with respect to this paper and are described in more detail in the following paragraphs. The signals from all of these transducers were digitized by a 16-bit A/D converter (National Instruments PCI-MIO-16XE-10) with a sampling rate of 1 kHz, and a set of typical measurements is shown in Fig. 2. In Fig. 2, the values for supply pressure and oxygen mass flow rate are averaged over 0.1 s, and the data include oxygen-to-fuel ratio (OFR).

Most of the results presented in this paper were obtained from analysis of the signal from the fast-response Kistler pressure transducer. The results are only concerned with the quasi-steady-state part of this signal, beginning immediately after the ignition pulse is stabilized and ending immediately before the initiation of shutdown. Typically the duration of this quasi-steady-state portion is around 8 s. The Kistler transducer has a natural frequency of 300 kHz, a sensitivity of 1.14 pC/psi (0.165 pC/kPa) and a linear range up to 15,000 psi (103.4 MPa). It was mounted 75 mm upstream of the fuel grain. A 100-mm-long fitting was used to reduce the exposure to the hot gases, which otherwise created an unacceptably high offset. This standoff fitting has its own resonance, but this was estimated to be at a higher frequency (825 Hz assuming a standing quarter-wave) than the range of 0–500 Hz considered in this paper.

A typical plume from the paraffin hybrid rocket is shown in Fig. 3. Plume flicker was quantified in terms of the signal from the Thorn EMI photomultiplier that received light emission from the entire plume. The light from the plume was collected and directed on to

the photomultiplier by a 28-mm lens with an aperture of ƒ1.8 that was located 15 m away from the combustor axis and at right angles to it. The photomultiplier signal was conditioned using an operational amplifier (National Semiconductor LF 411).

Calculation of the Instantaneous Port Diameter of the Fuel Grain

The amplitude spectrum of the chamber-pressure fluctuations typically contained three distinct peaks at around 30, 100, and 350 Hz, as seen in Fig. 4. In Fig. 4, normalized amplitude is defined as the rms of pressure fluctuations normalized by the mean pressure. The largest peak is that at around 30 Hz, and this frequency is less than any associated with geometric resonance. The peaks at around 100 and 350 Hz are associated with Helmholtz oscillations and a longitudinal acoustic wave (1-L mode) in the combustion chamber, respectively.[12] The rest of this section is concerned with the Helmholtz oscillation and, in particular, with determining the spatially averaged instantaneous port diameter of the fuel grain from the frequency measurements of this oscillation. The longitudinal-mode frequency is also used in the analysis to provide an estimate of the speed of sound in the combustion chamber.

Relationship Between the Helmholtz Oscillation and Fuel-Grain Port Diameter

A Helmholtz (bulk-mode) oscillation can occur whenever a large volume terminates in a narrow throat and is the same type of response that produces a tone when air is blown over the top of a bottle. Helmholtz oscillations occur due to the alternating compression and relaxation of the large volume by the fluid in the narrow throat. The natural frequency of this oscillation can be calculated as[13]

$$f = (c/2\pi)\sqrt{A/Vl} \tag{3}$$

For the present analysis, the relatively low-temperature incompressible fluid upstream of the beginning of the fuel grain is assumed to provide an unyielding boundary to the high-temperature low-density fluid downstream of it. Therefore, in the present configuration, the volume of the fluid that is compressed by the fluid in the nozzle throat, and, hence, that used to calculate the Helmholtz frequency, is equal to the sum of the fuel-grain port volume and the postcombustion-chamber volume.

Consistent with the inverse relationship between the Helmholtz frequency and the chamber volume, this frequency decreased monotonically as the port of the fuel grain opened up during the burn, as can be seen from the series of amplitude spectra of Fig. 5. In Fig. 5, normalized amplitude is defined as the rms of pressure fluctuations normalized by the mean pressure during the 1-s time interval being considered. A consequence of the continuous decrease in the frequency of the Helmholtz oscillation is that its amplitude that at any instant could exceed that of the 30 Hz oscillation (Fig. 5a) appeared small relative to the 30-Hz oscillation when the whole run is considered as in Fig. 4. This probably accounts for the fact that,

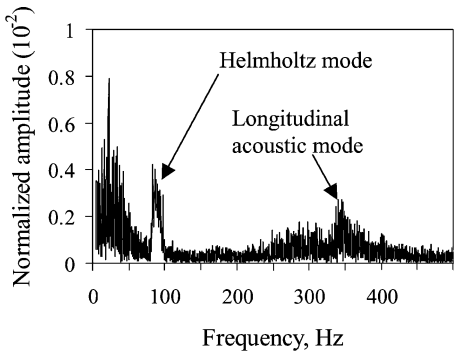

Fig. 4 Amplitude spectrum of the Kistler pressure transducer signal: P_{av} = 300 psi (2.07 MPa), $\dot{m}_{av}$ = 2.05 kg/s, OFR_{av} = 1.70, and D_0 = 0.090 m.

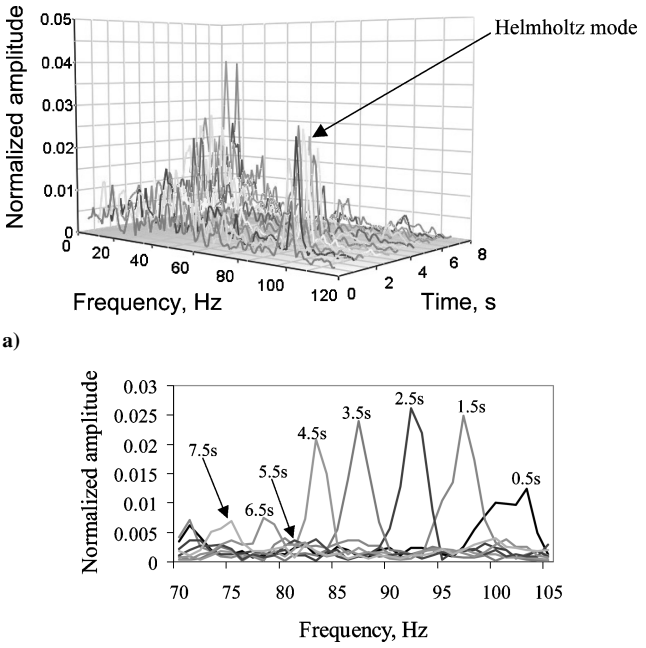

Fig. 5 Variation of pressure spectra with time, P_{av} = 300 psi (2.07 MPa), $\dot{m}_{av}$ = 2.05 kg/s, OFR_{av} = 1.70, and D_0 = 0.090 m; each spectrum is obtained over a 1-s interval and a) 0.5-s shift between adjacent spectra and b) 1-s shift between adjacent spectra.

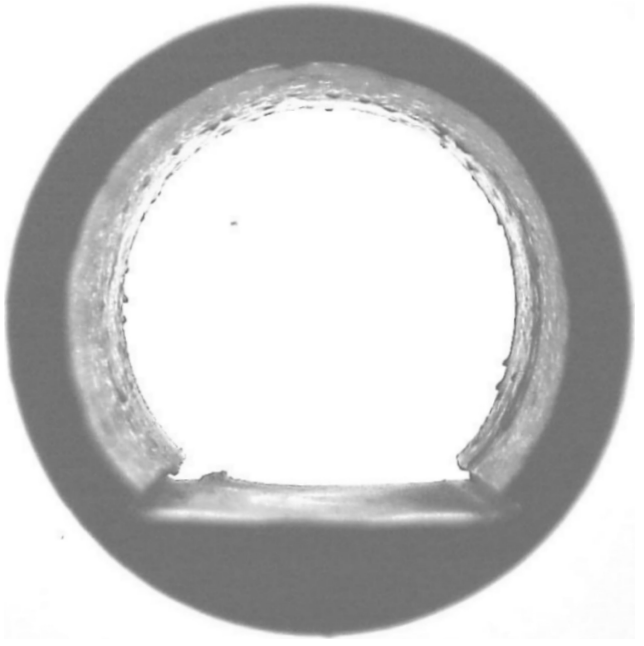

Fig. 6 Typical fuel grain after a test.

with few exceptions,[14] this mode of oscillation has not previously received any attention.

Examination of the paraffin fuel grain after a burn showed that the regression of the fuel is uniform along the axis (Fig. 6), with variations less than 5% even in the most extreme cases. It can be seen from Fig. 6 that the cross section is not circular but rather is flat along the bottom. This is due to the melted wax from the top and sides of the grain flowing down, pooling and solidifying on the bottom of the grain once the combustion is terminated. Thus, during operation, the grain is expected to be circular with uniform port diameter along the axis. Examination of the grain after a burn also showed that there had been little burning of the end faces of the fuel grain. Neglecting any burning on the end faces, the port

diameter along the length of the fuel grain is related to the chamber volume by

$$D = \sqrt{4(V - V')/\pi L} \tag{4}$$

Studies with other hybrid fuels[4,5] have shown variations of over 20% in fuel regression along the axis, and in this case the port diameter deduced from the chamber volume using Eq. (4) would provide a spatially averaged value.

When Eqs. (3) and (4) are combined, it can be seen that calculation of the instantaneous port diameter from the Helmholtz frequency requires estimating the instantaneous speed of sound in the combustor, as well as the instantaneous area and effective length of the nozzle throat. The following subsections provide estimates for these parameters.

Determination of the Nozzle Throat Area

The nozzle throat diameter was measured before and after the burn, and it was found to erode by less than 0.5%. For the present analysis, the throat area was assumed to change linearly between its initial and final values, and the uncertainty associated with this assumption is less than 0.2%. Therefore, at any time during the burn the throat area can be calculated as

$$A = (\pi/4)[d_0 + (t/t_{\text{tot}})(d_f - d_0)]^2 \tag{5}$$

Even the assumption that the nozzle throat diameter does not change during a burn will incorporate an error less than 1%. Note that application of this technique in real time will require the use of this assumption.

Determination of the Speed of Sound

The peak in the amplitude spectrum of the pressure fluctuations at around 350 Hz was determined, from tests with different motor lengths, to be a longitudinal half-wave in the motor.[12] This longitudinal-mode frequency changes during a burn, and its variation during two burns is shown in Fig. 7 together with linear fits through each set of frequencies. The two cases shown in Fig. 7 are those with the steepest and shallowest variation of frequency of those considered. The longitudinal-mode frequency used in the present analysis is that provided by the linear fit, and this differs from the instantaneous values by less than 5%. This is estimated to be the uncertainty in the measurement of this frequency.

The effective speed of sound in the motor at any instant can then be calculated from the longitudinal-mode frequency using

$$c = F\lambda = FL'/M \tag{6}$$

In the present configuration, the longitudinal mode is a half-wave, and hence, the acoustic-wave multiple M is equal to 0.5. Note that, because for the proposed technique it is the variation over time that is of interest, it is sufficient to consider the speed of sound as being proportional to the longitudinal-mode frequency and the constant of proportionality will be accounted when choosing the effective throat length as described in the following paragraph. Also note that application of this technique in real time requires the use of the instantaneous value of the longitudinal-mode frequency instead of a linear fit.

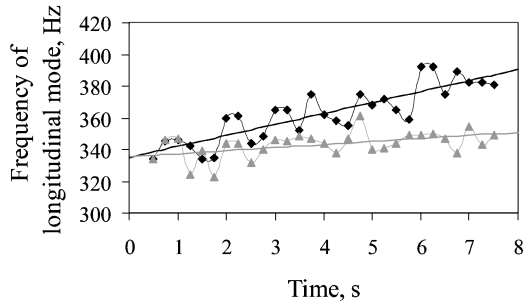

Fig. 7 Variation of longitudinal acoustic frequencies with time: ▲, $P_{\text{av}} = 300$ psi (2.07 MPa), $\dot{m}_{\text{av}} = 2.05$ kg/s, $\text{OFR}_{\text{av}} = 1.70$, and $D_0 = 0.090$ m; ◆, $P_{\text{av}} = 590$ psi (4.07 MPa), $\dot{m}_{\text{av}} = 5.55$ kg/s, $\text{OFR}_{\text{av}} = 2.89$, and $D_0 = 0.113$ m; and ——, linear fits through the data.

Determination of the Effective Nozzle Length

Definition of effective throat length is straightforward in configurations with a well-defined throat and is calculated as[13]

$$l = l' + 0.8d \tag{7}$$

Because the nozzle in the present study does not resemble the ideal configuration associated with Eq. (7), it is more difficult to define the effective throat length precisely. Therefore, the effective throat length was chosen such that the port diameter calculated from the Helmholtz frequency at the first measurement point corresponded to that calculated from Eq. (2) at the same time. The effective throat length was then assumed to remain constant at this value for the duration of the burn. The effective throat length was, thus, effectively used as a calibration constant and was defined by

$$l = \frac{\{F_1 L'[d_0 + (0.5/t_{\text{tot}})(d_f - d_0)]\}^2}{16\pi f_1^2 M^2 \left\{(\pi L/4)\left[a(2n+1)(4\dot{m}_1/\pi)^n + D_0^{2n+1}\right]^{2/(2n+1)} + V'\right\}} \tag{8}$$

where all of the parameters on the right-hand side of the equation are known or can be measured. Because of the use of a 1-s time interval to obtain the spectrum, the first frequency measurement was obtained 0.5 s into the burn.

Calculation of Port Diameter

Because the speed of sound, nozzle area, and effective throat length can be calculated as described earlier, the only unknown in Eq. (3) is the chamber volume. Thus, combining Eq. (3) with Eq. (4) provides the following expression for instantaneous port diameter in terms of the Helmholtz frequency:

$$D_{\text{s-av}} = \sqrt{\frac{4}{\pi L}\left[\left(\frac{F^2 L'^2 A}{4\pi^2 f^2 l M^2}\right) - V'\right]} \tag{9}$$

where all of the parameters on the right-hand side are known. $D_{\text{s-av}}$ was used instead of D in Eq. (9) for the expression to be applicable even when the regression is not uniform along the axis.

The technique presented for calculating the instantaneous port diameter was applied to a series of 10 tests. The profiles of instantaneous port diameter calculated at 0.25-s intervals for four of those tests are shown in Fig. 8 together with curve fits to these profiles that are represented by the broken lines. The unbroken lines shown in Fig. 8 represent the corresponding curves obtained from Eq. (2). It is clear that there is good agreement between this correlation and the profile of instantaneous port diameter deduced from the Helmholtz frequency. The arrows at the top right-hand corner of each graph indicate the port diameters determined by weighing the grains at the end of the burns, and these are in close agreement with the extraploations to the end of the runs of the port diameters calculated from the Helmholtz frequency.

Figure 9 shows a comparison of the port diameters calculated from the Helmholtz frequency with those obtained from equation (2) for all ten tests. It is clear that the difference between port diameters calculated by the two methods is less than 8% and, in fact, in most cases is less than 5%.

An uncertainty analysis following the constant-odds approach[15] was performed on the instantaneous port diameter calculated from Eq. (9), and the error bars are shown in Fig. 8. Of the parameters on the right-hand side of Eq. (9), the effective throat length, grain length, motor length, postcombustion-chamber volume, and acoustic-wave multiple are assumed to remain constant over the duration of the burn and, hence, do not contribute to the uncertainty in

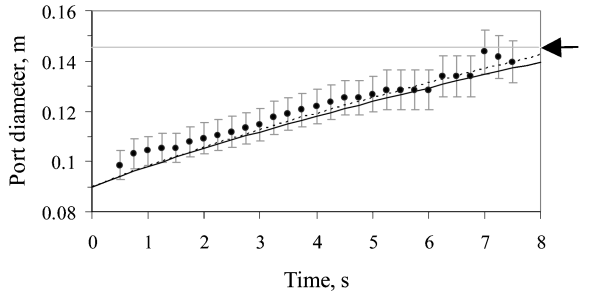

a) P_{av} = 300 psi (2.07 MPa), $\dot{m}_{av}$ = 2.05 kg/s, OFR_{av} = 1.70, and D_0 = 0.090 m

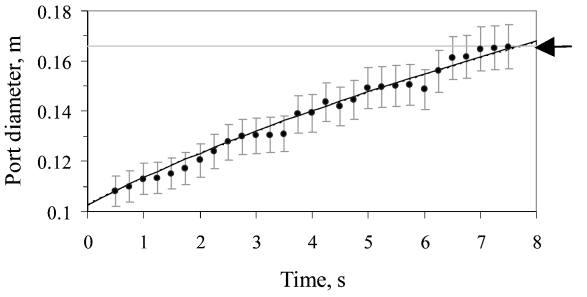

c) P_{av} = 540 psi (3.73 MPa), $\dot{m}_{av}$ = 4.46 kg/s, OFR_{av} = 2.71, and D_0 = 0.103 m

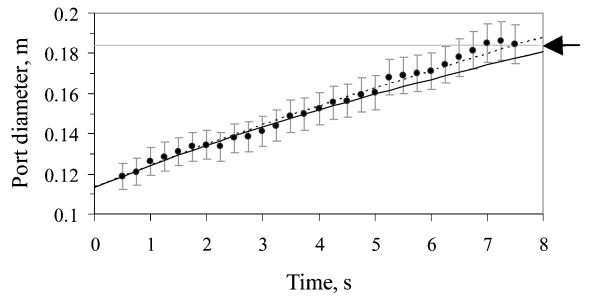

b) P_{av} = 590 psi (4.07 MPa), $\dot{m}_{av}$ = 5.55 kg/s, OFR_{av} = 2.89, and D_0 = 0.113 m

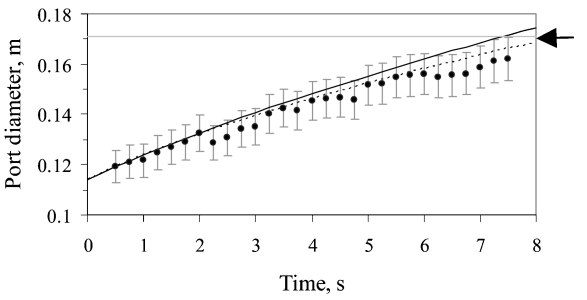

d) P_{av} = 602 psi (4.15 MPa), $\dot{m}_{av}$ = 4.44 kg/s, OFR_{av} = 2.77, and D_0 = 0.114 m, 10% by volume polyethylene mixed into the wax formulation

Fig. 8 Instantaneous port diameter: ●, port diameter calculated from the Helmholtz frequency; · · · ·, curve fits through these data points; ——, empirical correlation given by Eq. (2); and ←, port diameter measured at the end of burn.

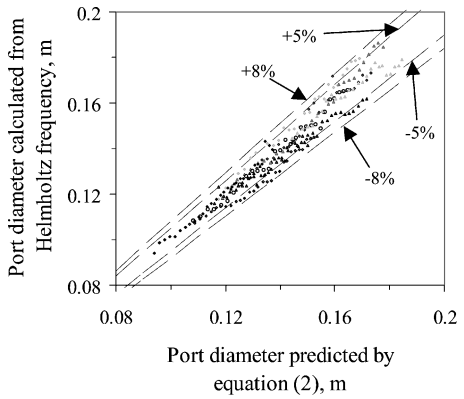

Fig. 9 Comparison of predicted port diameter.

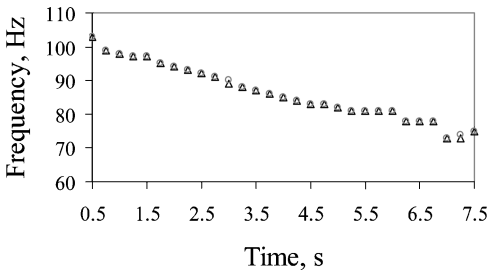

Fig. 10 Helmholtz frequency comparison, P_{av} = 300 psi (2.07 MPa), $\dot{m}_{av}$ = 2.05 kg/s, OFR_{av} = 1.70, and D_0 = 0.090 m: ○, frequencies obtained using the Kistler transducer and △, those using the photomultiplier.

calculating the variation of port diameter. Thus, the error bars indicated for the calculated port diameters in Fig. 8 incorporate uncertainties of ±5% in the estimated variation of the speed of sound and ±0.2% in the estimated variation of the nozzle area, as well as the uncertainty in measuring the Helmholtz frequency. The Helmholtz frequencies could in most cases be determined with an uncertainty of ±0.5 Hz. However, on some occasions, such as over the last 2 s shown in Fig. 8a, the peak associated with the Helmholtz oscillation diminished and became more difficult to distinguish, as can be seen from Fig. 5, and the uncertainty in identifying the Helmholtz frequency increased to ±2 Hz. The overall uncertainty in the calculated instantaneous port diameter is calculated by combining the independent uncertainties mentioned in this paragraph as follows:

$$\Delta D = \sqrt{\left(\frac{\partial D}{\partial f}\right)^2 (\Delta f)^2 + \left(\frac{\partial D}{\partial F}\right)^2 (\Delta F)^2 + \left(\frac{\partial D}{\partial A}\right)^2 (\Delta A)^2} \quad (10)$$

The maximum overall uncertainty in the calculated instantaneous port diameter was ±6.5%.

Note that the sensitivity of the technique, in terms of the change in Helmholtz frequency for a given change in port diameter, decreases with increasing port diameter due to the correspondingly smaller change in volume ratio. Despite this, the technique will be useful in larger motors as well because over the longer-duration burn typical of these motors the change in volume ratio is as large, if not larger, than in smaller motors.

The regression-rate profile can be deduced as the slope of the curve fit through the port diameters calculated from the Helmholtz frequency. It is clear from Fig. 8 that the regression rate decreased as the burns progressed and the ports opened up. As with techniques such as ultrasound and x-ray radiography that involve measurement of port diameter, deducing a more complete picture of instantaneous regression rate requires differentiation of the port-diameter profile with the introduction of additional uncertainties. Thus, further work to improve the accuracy of the proposed technique is required before the technique can be used to measure instantaneous regression rate.

Photomultiplier Measurements

Finally, the ability to obtain the same information about the fuel grain regression by observing the plume is considered. Spectral analysis of the signal from a photomultiplier that gathered light emission from the entire plume showed a peak corresponding to the Helmholtz frequency. The Helmholtz frequencies obtained from the photomultiplier signal are shown on Fig. 10, together with the corresponding values obtained with the high-speed pressure transducer. It is clear that there is good agreement between the two sets

of frequencies and, hence, that the photo-multiplier can be used to provide the same information regarding instantaneous port diameter as the pressure transducer.

Conclusions

This paper presented a technique for determining the instantaneous spatially averaged port diameter, and, therefore, regression rate, of the fuel grain in a hybrid rocket from analysis of a fast-response signal from a transducer measuring chamber pressure oscillations or from a photomultiplier observing the plume. In particular, this technique relied on analysis of the frequency of the Helmholtz oscillation of the combustor and was based on the principle that the Helmholtz frequency is inversely proporational to the square root of chamber volume. This technique was applied to a hybrid rocket burning gaseous oxygen and paraffin wax. The main conclusions follow.

1) The technique presented calculated the instantaneous port diameter of the paraffin fuel grain from measurements of the Helmholtz frequency with a maximum uncertainty of $\pm 6.5\%$.

2) This technique does not require any custom equipment, rather a high-speed pressure transducer that is typically an integral part of most rocket test facilities.

3) The measurement of plume flicker with a photomultiplier provides faithful representation of the frequency of the Helmholtz oscillations and, thus, can be used instead of the pressure transducer in a nonintrusive application of the technique.

Acknowledgments

This work was performed while Shane De Zilwa held a National Research Council Research Associateship at the NASA Ames Research Center. Useful discussions with Brian Cantwell, Rabindra Mehta, and James Ross are gratefully acknowledged.

References

[1]Marxman, G. A., Wooldridge, C. E., and Muzzy, R. J., *Fundamentals of Hybrid Boundary Layer Combustion*, Progress in Astronautics and Aeronautics, Vol. 15, AIAA, New York, 1964, pp. 485–521.

[2]Smoot, L. D., and Price, C. F., "Regression Rate of Nonmetallized Hybrid Fuel Systems," *AIAA Journal*, Vol. 3, No. 8, 1965, pp. 1408–1413.

[3]Smoot, L. D., and Price, C. F., "Pressure Dependence of Hybrid Fuel Regression Rates," *AIAA Journal*, Vol. 5, No. 1, 1967, pp. 102–106.

[4]George, P., Krishnan, S., Varkey, P. M., Ravindran, M., and Ramachandran, L., "Fuel Regression Rate in Hydroxil-Terminated-Polybutadiene/Gaseous Oxygen Hybrid Rocket Motors," *Journal of Propulsion and Power*, Vol. 17, No. 1, 2001, pp. 35–42.

[5]Chiaverini, M. J., Serin, N., Johnson, D. K., Lu, Y. C., Kuo, K. K., and Risha, G. A., "Regression Rate Behavior of Hybrid Rocket Solid Fuels," *Journal of Propulsion and Power*, Vol. 16, No. 1, 2000, pp. 125–132.

[6]Wernimont, E. J., and Heister, S. D., "Reconstruction Technique for Reducing Hybrid-Rocket Combustion Test Data," *Journal of Propulsion and Power*, Vol. 15, No. 1, 1999, pp. 128–136.

[7]Karabeyoglu, M. A., Zilliac, G., Cantwell, B., De Zilwa, S. R. N., and Castellucci, P., "Scale-Up Tests of High Regression Rate Liquefying Hybrid Rocket Fuels," AIAA Paper 2003-1162, Jan. 2003.

[8]Karabeyoglu, M. A., Cantwell, B., and Altman, D., "Combustion of Liquefying Hybrid Propellants, Part 1: General Theory," *Journal of Propulsion and Power*, Vol. 18, No. 3, 2002, pp. 610–620.

[9]Russo Sorge, A., and Carmicino, C., "Pressure and Temperature Effect on Regression Rate Measurements by an Ultrasonic Transducer in a Hybrid Rocket," *Proceedings of the 3rd TEMPE-ISAS Joint Workshop on Space Propulsion and Related Materials*, Bonassola, Italy, June 2001.

[10]Korting, P. A. O. G., Schoyer, H. F. R., and Timnat, Y. M., "Advanced Hybrid Rocket Experiments," *Acta Astronautica*, Vol. 15, No. 2, 1987, pp. 97–104.

[11]Evans, B., Risha, G. A., Favorito, N., Boyer, E., Wehrman, R. B., Libis, N., and Kuo, K. K., "Instantaneous Regression Rate Determination of a Cylindrical X-Ray Transparent Hybrid Rocket Motor," AIAA Paper 2003-4592, July 2003.

[12]De Zilwa, S., Karabeyoglu, A., Zilliac, G., Reinath, M., and King, L., "Combustion Oscillations in High Regression Rate Hybrid Rockets," AIAA Paper 2003-4465, July 2003.

[13]Crighton, D. G., Dowling, A. P., Ffowcs Williams, J. E., Heckl, M., and Leppington, F. G., "Resonators," *Modern Methods in Analytical Acoustics*, Springer-Verlag, Berlin, 1992, pp. 572–575.

[14]Pucci, J. M., "The Effects of Swirl Injector Design on Hybrid Flame-Holding Combustion Instability," AIAA Paper 2002-3578, July 2002.

[15]Holman, J. P., "Analysis of Experimental Data," *Experimental Methods for Engineers*, McGraw–Hill, New York, 1978, pp. 43–51.